Journal of Materials Chemistry A

ROYAL SOCIETY OF CHEMISTRY

PAPER

View Article Online
View Journal

Cite this: DOI: 10.1039/d6ta03607d

Spectroscopic investigation of the electrochemical growth and stability of am-hydr-IrO_x grown from IrTi alloys

Benjamin Howchen, *[a] Marianne van der Merwe, [a] Alexander Steigert,[b] Raul Garcia-Diez, [a] Catalina E. Jimenez, [ac] Rosario Suarez Anzorena, [ad] Roberto Félix, [ac] Ilaria Lucentini, [ef] Carlos Escudero, [e] Johannes Frisch,[ac] Regan G. Wilks [ac] and Marcus Bär *[acgh]

Amorphous hydrous iridium oxide thin films (am-hydr-IrO_x) grown through electrochemical treatment of sputtered iridium thin films are an interesting class of materials for the oxygen evolution reaction (OER). They boast high electrochemical activity and high mass utilisation of the precious metal iridium; however, the application of am-hydr-IrO_x is limited by poor stability caused by film delamination and electrochemically enhanced corrosion. This study presents a comprehensive investigation of the behaviour of am-hydr-IrO_x grown from co-sputtered iridium with titanium (IrTi) films. The growth behaviour of IrTi films is investigated in detail by employing X-ray photoelectron spectroscopy, which enables unique insights into the structure and mechanism of the resultant am-hydr-IrO_x species. Depth-dependent hard X-ray photoelectron spectroscopy (HAXPES) experiments using different excitation energies show that the films separate into an iridium rich hydrous oxide layer supported by an unreacted metallic alloy during growth. Complementary element specific *operando* X-ray absorption spectroscopy studies at the Ir L_3- and Ti K-edges in combination with electrochemical techniques are further used to ascertain details of the growth mechanisms and develop a hypothesis to connect the electrocatalyst structure to its electrochemical stability under hydrolysis-relevant conditions. Titanium oxide formation at the surfaces acts to impede the formation of am-hydr-IrO_x, and above a critical concentration, the presence of titanium results in an impressive stability enhancement.

Received 29th April 2026
Accepted 22nd May 2026

DOI: 10.1039/d6ta03607d

rsc.li/materials-a

1. Introduction

Proton exchange membrane water electrolysers (PEM-WEs) are considered to be one of the leading technologies for industrial scale water splitting.[1,2] However, widespread use is limited by the stability of electrocatalyst materials to drive the oxygen evolution reaction. Due to the harsh, highly oxidizing, and low pH conditions, PEM-WE anodes typically utilise materials containing precious metals such as iridium.[3] The employment of water electrolysis involves coupling of intermittent renewable energy sources with electrolysers.[4] As a result, electrocatalysts need to be stable also under (to some degree) fluctuating operation schemes. There are several different proposed mechanisms that contribute to the performance loss of iridium-based electrocatalyst materials, each contributing to different extents, based on the electrocatalyst's electronic and crystal structure.[5] For example, potential dependent dissolution mechanisms such as the formation of highly soluble, high valence iridium (Ir^{VI}) species[6] or low coordinated iridium sites *via* lattice oxygen evolution have been proposed.[7] Other processes detrimental to the performance of Ir-based anode electrocatalysts are the poorer electronic conductivity of the electrocatalyst after prolonged operation due to discontinuities in the supported active layer[8] or the increased contact resistance with the Ti-based porous transport layer.[9]

Lately, amorphous, hydrous iridium oxides (am-hydr-IrO_x) have caught attention for acidic water electrolysis due to their high activity, high iridium active site availability and acid

[a]*Interface Design, Helmholtz-Zentrum Berlin für Materialien und Energie GmbH (HZB), Albert-Einstein-Str. 15, Berlin 12489, Germany. E-mail: marcus.baer@helmholtz-berlin.de*

[b]*PVComB, HZB, Schwarzschildstr. 3, Berlin 12489, Germany*

[c]*Energy Materials* In-Situ *Laboratory Berlin (EMIL), HZB, Albert-Einstein-Str. 15, Berlin 12489, Germany*

[d]*Unidad de Investigación y Desarrollo Estratégico para La Defensa (UNIDEF-CONICET-MINDEF), CITEDEF, J.B. de La Salle 4397, B1603ALO Villa Martelli, Buenos Aires, Argentina*

[e]*ALBA Synchrotron Light Source, Carrer de La Llum 2-26, Cerdanyola Del Vallès, Barcelona 08290, Spain*

[f]*Department of Chemical Engineering, Universitat Politècnica de Catalunya, EEBE, Eduard Maristany 10-14, Barcelona 08019, Spain*

[g]*Department of Chemistry and Pharmacy, Friedrich-Alexander-Universität Erlangen-Nürnberg (FAU), Egerlandstr. 3, Erlangen 91058, Germany*

[h]*Helmholtz-Institute Erlangen-Nürnberg for Renewable Energy (HI ERN), Albert-Einstein-Str. 15, Berlin 12489, Germany*

tolerance.[10–12] The am-hydr-IrO_x structures can be generated through electrochemical cycling of metallic iridium substrates generating a highly porous, hydrated iridium oxide layer.[13–15] However, compared to crystalline iridium oxide, am-hydr-IrO_x suffers from poorer stability due to the thermodynamically driven dissolution of the active metal at high overpotentials and low pH.[16–19] In addition, recent work predicts Ir dissolution in am-hydr-IrO_x by spontaneous formation of iridium vacancies occurring at potentials as low as 0.9 V *vs.* the reversible hydrogen electrode (RHE).[20]

Mechanical stability of the porous film can be influenced by excessive growth of am-hydr-IrO_x, where the gas evolution in the porous oxide network can lead to partial or total delamination of the active area from the metallic Ir substrate.[21,22] Mechanical stability is particularly relevant for am-hydr-IrO_x, as varying voltage from intermittent renewable energy sources coupled to the PEM-WE could lead to further undesirable growth and eventual delamination of the electrocatalyst layer. To improve their stability, many active anode materials are combined with acid-stable oxides either as a support or by partial substitution into the crystal lattice. Oxides of titanium and tin are particularly popular, showing improved stability against dissolution and having positive synergies in combination with iridium.[23–25] However, as they are inactive towards the OER, their combination with active materials often comes at the cost of lower performance.[24,26–28] A more profound understanding of the interaction between, *e.g.* titanium and iridium in its amorphous hydrous form may lead to strategies to stabilize the highly catalytic am-hydr-IrO_x.

In this work, we investigate the behaviour of hydrous iridium oxide thin films grown from alloys of iridium and titanium of various compositions. The complex growth behaviour of the highly hydroxylated porous electrocatalysts requires characterisation at various stages of the life of the electrocatalyst film. Here, lab-based and synchrotron-based advanced X-ray spectroscopic methods were used to provide depth-resolved information on the chemical composition of the films as they evolve throughout the electrochemically induced growth procedures. In addition to thorough spectroscopic characterisation of the films, the activity and stability of the films were studied and evaluated using a variety of electrochemical techniques. With these results, the role of titanium in the vicinity of iridium atoms during the electrochemical growth of am-hydr-IrO_x is thoroughly investigated for different Ti concentrations, aiming to reveal the processes triggered by titanium that can improve the stability of iridium-based OER electrocatalysts.

2. Results

2.1 Characterisation of the pristine IrTi alloy films

Thin films of IrTi alloys were prepared by co-sputtering iridium and titanium onto silicon wafers, yielding surface metal elemental ratios ranging from pure iridium (Ir_{100}) to 74 at% Ir ($Ir_{74}Ti_{26}$). These elemental surface ratios were derived from the Ti 2p (including metallic and oxidised species) and Ir 4f X-ray photoelectron spectroscopy (XPS) detail spectra shown in Fig. 1a and b. Note that the Ir 4f spectra overlap with the Ti 3s and Ir $5p_{1/2}$ core level lines,[23] but their spectral contributions are considered to be negligible when probed with Al K_α, as in this case their photoionization cross sections are more than one order of magnitude smaller than that of Ir 4f. Details on the quantification of the XPS data are described in the SI (Fig. S4 and Table S1). Fig. S2 shows the survey spectra of the pristine films with the different photoemission lines of the constituent elements labelled. The Ti 2p core level spectra show that titanium exists in multiple chemical states dominated by metallic Ti and oxidised Ti species (Fig. 1a). This observation is consistent with previous reports.[23] The ratio of metallic and oxidised titanium species varies throughout the samples whereby samples with high total titanium content have higher relative proportions of oxidised Ti species. This was quantified by deconvolution of the Ti 2p spectra (Fig. S6) and the relationship with respect to the elemental surface ratio is shown in Fig. S7. The Ir 4f spectra show a shift towards lower binding energies with increasing titanium concentration (Fig. 1b), supporting the argument that a solid solution type alloy is also being formed. Similar effects have been reported with a shift of up to 4 eV to lower binding energies for an equimolar composition.[30] Although, by analogy, a shift up to 2 eV could be expected between Ir_{100} and $Ir_{74}Ti_{26}$, we only observe a shift of ≈ -0.5 eV, consistent with the scenario that parts of the titanium are not completely incorporated into the lattice but are segregated within the iridium matrix, thus, not contributing to the chemical shift of Ir 4f.

X-ray reflectometry indicates a rather uniform film thickness of 33 ± 4 nm for all films independent of Ti content (see Fig. S5 and Table S2). Phase purity and crystal structure of the pristine films were determined with grazing incidence X-ray diffraction (GI-XRD) as shown in Fig. 1c. It is observed that the addition of titanium into the iridium lattice results in a shift of the main Ir (111) reflection to higher angles, from 40.5° (Ir_{100}) up to 40.9° ($Ir_{74}Ti_{26}$). This is consistent with the successful formation of an alloy, where the introduction of a smaller-radius element leads to a decrease in the associated lattice parameter; however, strain effects in the thin films cannot be excluded. The latter (more specifically directional lattice strain) could also explain why at higher titanium concentrations the more prominent Ti (002) reflex associated with the titanium alpha phase is observed at around 38° (as expected) while the Ti (101) reflex is significantly shifted to higher angles and observed at 43°.[29] The appearance of the peaks in GI-XRD is related to the segregation of a long-range ordered titanium phase (which could be a nanocluster in the alloy, although a segregated phase at the surface could not be excluded). Alloys can be understood as either (a) solid solutions, where there is a single crystal structure with multiple elements occupying the crystallographic sites, or, alternatively, (b) a mixture of two or more metallic phases, where one forms a sub-structure within the parent phase.[30] For these IrTi thin film materials, it appears that both types of alloys are simultaneously present and, therefore, the metallic pristine IrTi films will be referred to as alloys.

2.2 Electrochemical growth from the IrTi alloy films

The am-hydr-IrO_x electrocatalyst layers were grown from their respective metallic IrTi alloy films using methodology reported

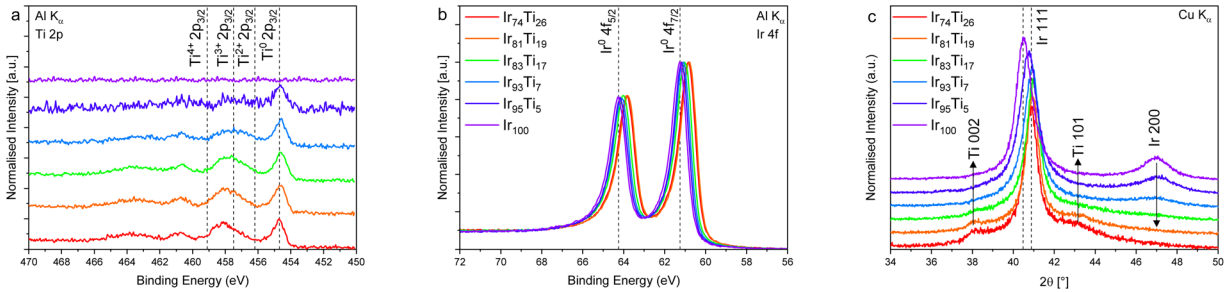

Fig. 1 Characterisation of pristine films. (a) Al K_α (1486.71 eV) excited Ti 2p XPS detail spectra of IrTi films with varying compositions (see the colour code); dotted vertical lines highlight the reference binding energies of the Ti $2p_{3/2}$ line, consisting of metallic titanium (Ti^0) and oxidised titanium species (Ti^{2+}, Ti^{3+}, and Ti^{4+}). (b) Corresponding Al K_α excited Ir 4f XPS detail spectra; dotted vertical lines represent the reference binding energies of the spin–orbit doublet of the Ir 4f line for metallic iridium (Ir^0). (c) Grazing incident X-ray diffraction patterns (GI-XRD); dotted vertical lines highlight the shift in peak position of the Ir (111) reflex between the Ir_{100} and the $Ir_{74}Ti_{26}$ sample. Arrows highlight the decrease of the Ti (002) and (101) reflexes with increasing iridium content and the appearance of a secondary iridium reflection.

elsewhere.[12] In brief, the IrTi alloys were voltametrically cycled between reductive and oxidative potentials at 500 mV s^{-1} up to 1000 total cycles.[15] After every increment of 200 cycles, a cyclic voltammogram (CV) was measured at a slower rate (10 mV s^{-1}). The slow CVs of the compositional extremes of the IrTi alloy films, $Ir_{74}Ti_{26}$ and Ir_{100}, are shown in Fig. 2a and b respectively, illustrating a significant difference in the growth behaviours, where the pure iridium sample (Ir_{100}) exhibits a significantly higher growth rate than its alloy counterpart ($Ir_{74}Ti_{26}$, the complete set of electrochemical profiles is shown in Fig. S9). This is seen in the increase in the capacitance and pseudocapacitive-redox with respect to cycle number, highlighted by the arrows in panels (a) and (b) of Fig. 2. This growth reflects an increased surface area with an increased number of electrochemically available iridium sites.

To study this effect further, the areas of the redox features were quantified by integrating the reductive portion of the peak around 0.95 V *vs.* RHE to avoid influence from the small redox feature seen around 0.7 V *vs.* RHE. The number of electrochemically available sites was estimated from the charge, which was calculated from the area of the redox feature and is plotted as a function of cycle number in Fig. 2c. The area of the redox feature was derived using a linear background to remove capacitive effects between 0.6 and 1.2 V *vs.* RHE. A clear relationship is observed between the rate of growth with respect to the number of electrochemical growth cycles and the elemental composition. An increasing titanium content apparently prevents the participation of iridium sites in the electrochemical growth (limiting it), as interpreted from the reduced voltametric charge. This results into a slower growth rate for the films with higher Ti content, as documented by the smallest voltametric charge observed for the $Ir_{74}Ti_{26}$ thin film. For simplicity, the different numbers of electrochemically available iridium sites, *i.e.* sites within the am-hydr-IrO_x electrocatalysts grown from the different alloy films, will be referred to as "thickness" but this does not necessarily describe a closed layer supported by the metal sublayer. However, it has been shown to linearly correlate with film thickness.[20] Despite titanium having a clear impact on the growth rate of the amorphous hydrous layer, it does not show direct effects on the electrochemical signature of the amorphous hydrous iridium oxide, reflected by the feature around 0.95 V *vs.* RHE observed in all samples. A similar shift of the small anodic peak found around 0.7 V *vs.* RHE as a function of the growth is observed in all samples, as seen in Fig. S9.

2.3 Depth-dependent chemical analysis of 1000-cycle grown am-hydr-IrO_x layer films

To probe the chemical composition of the different alloy films grown up to 1000 cycles, they were studied using hard X-ray

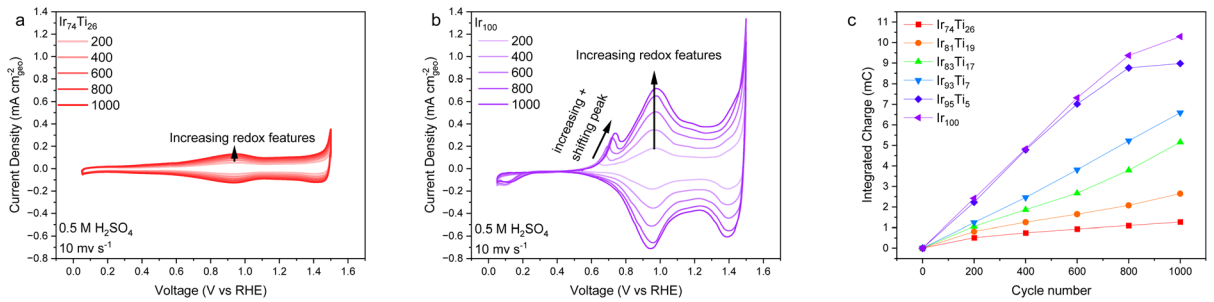

Fig. 2 Electrochemically induced growth behaviour measured by cyclic voltammetry at 200, 400, 600, 800 and 1000 cycles at a scan rate of 10 mV s^{-1} in 0.5 M H_2SO_4 during the 1000-cycle growth of (a) the $Ir_{74}Ti_{26}$, and (b) the Ir_{100} thin film. (c) Quantified growth behaviour for all studied IrTi films of varying Ti content derived from the integral of the pseudocapacitance of the observed reductive peak at ≈ 0.95 V *vs.* RHE as a function of cycle number.

photoelectron spectroscopy (HAXPES) at the HiKE endstation.[31] Fig. 3a shows the Ir 4f spectra of the samples measured with 2 keV, with pristine $Ir_{74}Ti_{26}$ as a reference. Dashed lines highlight the positions of the Ir $4f_{7/2}$ contributions for both IrO_2 and metallic iridium. All samples show only evidence of oxidised iridium except for am-hydr-IrO_x grown from $Ir_{74}Ti_{26}$, which also shows peaks associated with metallic iridium. The Ir 4f region was also measured using a higher excitation energy (6 keV), as shown in Fig. 3b, and, therefore, with a higher probing depth. These less surface-sensitive measurements revealed more unreacted metallic iridium, hinting at a layered structure where the am-hydr-IrO_x grows on top of the unreacted parts of the

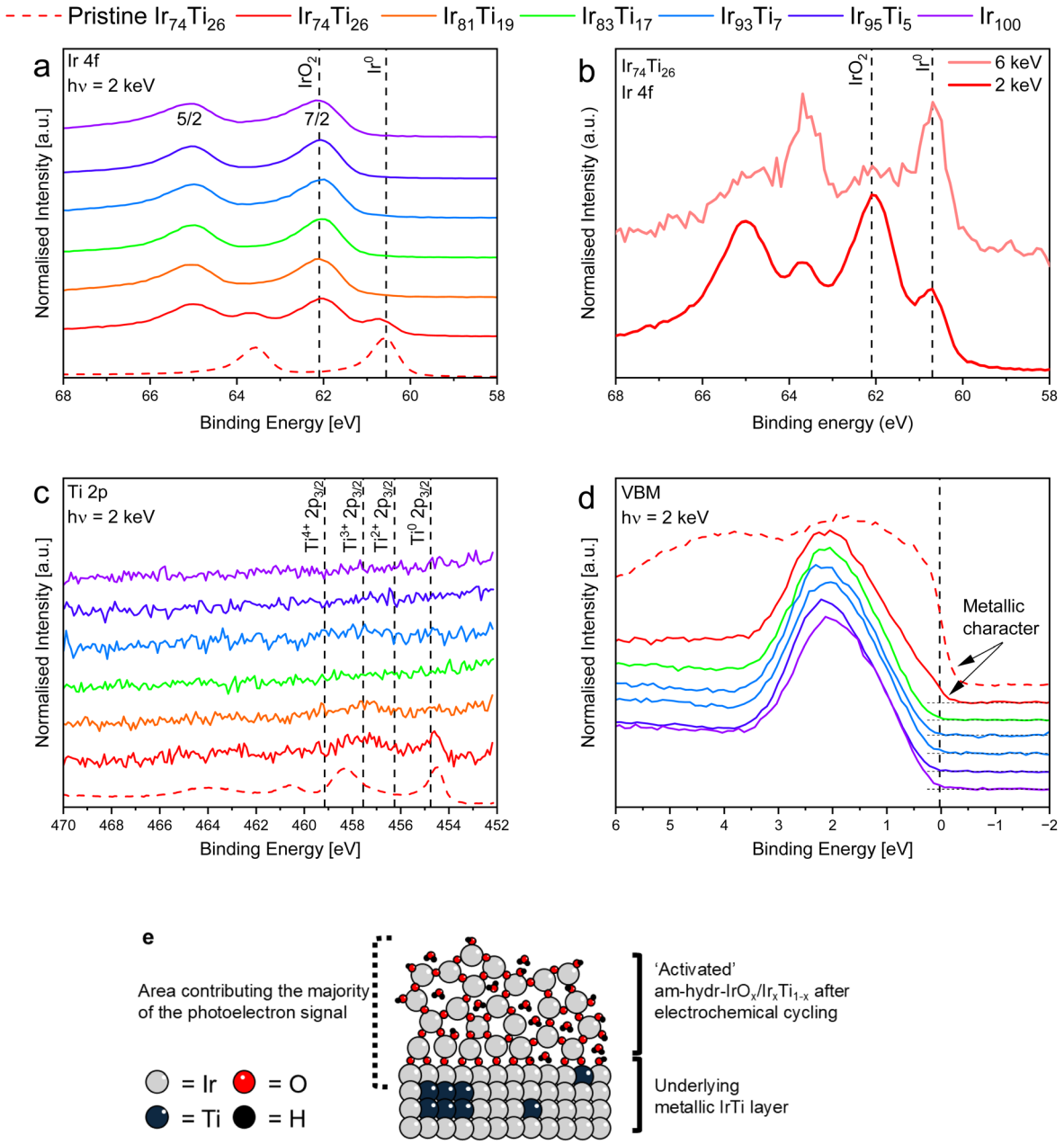

Fig. 3 Hard X-ray photoelectron spectroscopy of 1000-cycle grown am-hydr-IrO_x (a) Ir 4f HAXPES detail spectra recorded at 2 keV excitation energy. The dotted lines highlight the Ir $4f_{7/2}$ binding energy position of metallic and oxidized iridium. (b) Ir 4f spectra of the am-hydr-IrO_x layer grown on the $Ir_{74}Ti_{26}$ alloy film (*i.e.*, the sample with the highest surface titanium content in the pristine alloy film), measured with both 2 and 6 keV. The dotted lines highlight the Ir $4f_{7/2}$ binding energy position of metallic and oxidized iridium. (c) Ti 2p spectra recorded with an excitation energy of 2 keV. The dotted lines highlight the Ti $2p_{3/2}$ binding energies for metallic titanium (Ti^0) and oxidised species. (d) HAXPES spectra of the valence band maxima. The vertical dotted line indicates the position of the Fermi level (0 eV binding energy). (e) Schematic of the structural model proposed within this work, whereby the am-hydr-IrO_x layer grows from the IrTi films and is the major contributor to the HAXPES signal, except for the sample with the thinnest am-hydr-IrO_x top layer ($Ir_{74}Ti_{26}$). For this sample, the contribution from the metallic alloy layer is clearly observed in the HAXPES data.

alloy film. Note that the Ir 4f spectra overlap with the Ti 3s and Ir $5p_{1/2}$ core level lines,[23] but their spectral contributions are considered to be negligible when probed with 2 keV (see explanation above). However, for the 6 keV excited Ir 4f spectra, Ti 3s and Ir $5p_{1/2}$ derived spectral contributions have to be considered (especially when quantifying the data), but this does not affect the qualitative statement that more unreacted metallic iridium is present in the less surface-sensitive measurements made above.

Considering that the HAXPES detection limit is between 0.1 and 1 at% (depending on the photoionization cross section of the probed core level), it is worth noting that a Ti 2p HAXPES signal is only detected for the am-hydr-IrO_x film grown from the $Ir_{74}Ti_{26}$ film (Fig. 3c). This suggests that Ti is largely absent from the grown am-hydr-IrO_x layer and the fact that Ti is only detected for the $Ir_{74}Ti_{26}$ based film can be explained by considering the am-hydr-IrO_x layer grown from the $Ir_{74}Ti_{26}$ film as the thinnest one (see Fig. 2c).

To support this hypothesis, HAXPES detail spectra of the valence band maximum (VBM) were also studied to see if there were any significant electronic differences in the am-hydr-IrO_x grown from IrTi alloy films with different compositions, since small amounts of titanium could influence the electronic structure while not being directly detectable. Fig. 3d shows the measured data of the grown am-hydr-IrO_x films, with the pristine $Ir_{74}Ti_{26}$ film also included as a reference.

All am-hydr-IrO_x layers again show very similar spectral valence band features, except for the one grown from the $Ir_{74}Ti_{26}$ film having a shallower slope of the leading valence band edge resulting in significant spectral intensity above the Fermi level (highlighted by arrows in Fig. 3d), as can be also observed for the corresponding pristine film, although significantly more pronounced. This further supports the hypothesis that am-hydr-IrO_x grown from the alloy films presumably contains little to no titanium, which leads to the question of whether the titanium is lost during the electrochemical growth.

In order to study this, X-ray absorption spectroscopy (XAS) at the Ti K-edge with a higher probing depth (0.5 to 1 μm in fluorescence yield[32]) was performed. All 1000-cycle samples show similar spectra, as depicted in Fig. S11a. The spectral fingerprint in these samples, characteristic of metallic Ti^0 mixed with that of titanium oxides in smaller concentrations, is also comparable to the spectra of the pristine IrTi alloy films. This confirms that titanium dissolution presumably does not explain the HAXPES-derived titanium-poor composition of the 1000-cycle grown am-hydr-IrO_x. This follows chemical intuition as titanium is a very corrosion resistant material, due to the non-porous protective oxide coating formed in the presence of acids.[33] Based on the HAXPES and XAS data, a model illustrated in Fig. 3e is proposed, where am-hydr-IrO_x grows from the alloy films and covers the entire surface but contains little to no titanium, supported on unreacted metallic alloy, leading to an am-hydr-IrO_x/Ir_xTi_{1-x} layer stack. Only for the thinnest film can the underlying alloy be detected by HAXPES, while, for all others, the spectroscopic signals observed originate solely from am-hydr-IrO_x.

2.4 Electrochemical OER activity of the 1000-cycle am-hydr-IrO_x grown from IrTi alloy films

The cyclic voltammograms corrected for voltage errors caused by solution resistance (R) and current flow (i) highlighting the electrochemical activity towards the oxygen evolution reaction are compared in Fig. 4a. The series resistances were determined by first growing the am-hydr-IrO_x layer up to 1000 cycles, measuring the impedance spectrum and then extracting the high frequency response. The series resistance of the 1000-cycle am-hydr-IrO_x layers is a function of the elemental composition of the alloy films as highlighted in Fig. 4b, whereby the series resistance decreases with higher iridium content in the initial alloy film. After iR correction, the similarity in activities between the different samples is somewhat counterintuitive, since thickness, *i.e.* the number of electrochemically active sites derived from the voltametric charge, varies with the metal composition of the film as shown in the inset in Fig. 4a. All evidence up to this point suggest that the catalytic activity of all 1000-cycle am-hydr-IrO_x layers grown from IrTi alloy films

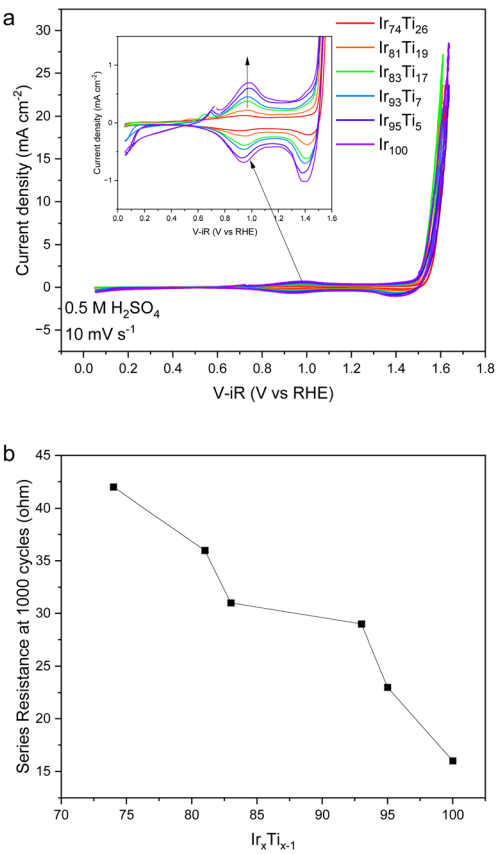

Fig. 4 Electrochemical activity of 1000-cycle am-hydr-IrO_x layers grown from IrTi alloys with different Ir contents: (a) iR compensated cyclic voltammetry. The inset shows an enlarged portion of the cyclic voltammograms highlighting differences in the capacitance between samples. All cyclic voltammograms were measured at 10 mV s^{-1} and the current is normalized by the geometric surface area of the sample. (b) Series resistance of the different 1000-cycle am-hydr-IrO_x layers grown on IrTi alloys with different surface iridium contents. The series resistance was derived from the high frequency response in impedance measurements.

(containing mostly, if not exclusively, iridium as the metal) is very similar, differing only with respect to their thicknesses. In OER electrocatalysis, it is typically assumed that, for the same active site, activity should linearly correlate with the number of active sites (*e.g.*, their total quantity). To probe this relationship for the am-hydr-IrO_x samples studied, the activity of corresponding layers grown from Ir_{100} as a function of cycles was studied and is shown in Fig. S14. A direct correlation between the activity of the sample and its integrated charge (the proxy measurement for electrochemically active sites) should be observed; however, the results are significantly more complex. Fig. S14a shows the cyclic voltammograms of the am-hydr-IrO_x layers grown on Ir_{100} as a function of cycle number, with the inset highlighting the growth of the am-hydr-IrO_x layer *via* the increase in (pseudo)capacitance of the redox features. The OER activity is measured by the current density at 1.7 V *vs.* RHE and is plotted against the integrated charge of the redox feature in Fig. S14b. From this, it can be derived that the relationship between the number of electrochemically active sites and activity is clearly not direct. Although we see an initial increase in activity between the first 200–400 cycles, this does not follow the steady increase in the redox integral. At high cycle numbers, we see a large drop in activity, coinciding with a small decrease in am-hydr-IrO_x layer thickness. A detailed interpretation of this observation is developed further in the discussion section below. An alternative explanation for similar *iR* corrected electrochemical activities across the samples, despite the different numbers of exposed catalytic sites, could be due to subtle changes in the electronic structure of the active iridium sites caused by proximal titanium. The electrochemical signature of iridium shown in Fig. 4 and S9 does not appear to reflect any Ti content related changes in the electronic structure of iridium, but rather just shows the extent of am-hydr-IrO_x growth (thickness). However, this possibility was studied further using *operando* X-ray absorption spectroscopy of the Ir L_3-edge with details of the experimental procedure found in the SI. After being grown up to 1000 cycles, the am-hydr-IrO_x layers were held at several voltages where key electrochemical events occur across the pre-catalytic voltage range and the absorption spectra were recorded, as shown in Fig. S15. It was observed that, within the error of the measurement, all samples that were measured exhibited similar white line position shifts as a function of voltage, supporting the conclusions drawn from the electrochemical experiments that electrochemical activity is dominated by the active iridium atoms within the sample and providing evidence that the active species in all samples is am-hydr-IrO_x, revealed to grow with almost no Ti on top of the remaining unreacted parts of the alloy film.

2.5 Electrochemical stability

To study how the initial composition of the IrTi alloy influences the stability of the am-hydr-IrO_x grown from it, different accelerated testing protocols were utilised to highlight the differences in sensitivity to the different degradation mechanisms between the alloy films. The electrocatalysts were subjected to two different potential regimes. The stability towards cycle-induced delamination was evaluated by cycling 10 000 times using the typical growth parameters at a scan rate of 500 mV s^{-1} with a slower scan of 50 mV s^{-1} at increments of 1000 cycles to track changes in the voltametric response. This aims to mimic shut down/switch on protocols, ranging from very high to low potentials within seconds, while limiting potential-induced dissolution by minimising the time spent in a potential range where minimal OER occurs. In contrast, the stability towards potential-induced dissolution was studied potentiostatically at a voltage where OER readily occurs and minimal further growth of am-hydr-IrO_x is expected. Fig. 5a and b show voltammograms of Ir_{100} and $Ir_{74}Ti_{26}$ films treated to 1000 and 10 000 cycles, respectively. Ir_{100} exhibits a dramatic change resulting from this electrochemical procedure; the loss of the capacitive current is consistent with the loss of electrocatalytically active iridium oxide material since electrochemically active iridium contributes to the (pseudo)capacitive current. In addition, the change in voltametric response indicates a chemical change in the electroactive species. In contrast, the $Ir_{74}Ti_{26}$ alloy film only shows subtle changes in the positions and shape of its electrochemical fingerprint, suggesting maturation of the film but not severe destruction, as seen previously for the pure iridium system. The chemical composition of the am-hydr-IrO_x films after 10 000 cycles was further studied using XPS/HAXPES and compared to measurements of pristine alloy films and am-hydr-IrO_x samples grown to 1000 cycles, as shown in Fig. 5c–f. In the pristine $Ir_{74}Ti_{26}$ film, iridium is in its metallic state. After 1000 cycles, photoemission lines corresponding to oxidized and metallic iridium are observed (see Ir 4f spectra in Fig. 5c). These originate from the surface am-hydr-IrO_x grown from the alloy film and the unreacted alloy underneath. At the same time, the Ti 2p region (Fig. 5e) shows both oxidized and metallic components in the pristine film. Deviation from expected binding energies was ascribed to localised charging of insulating TiO_2 species. After 1000 cycles, no major changes in the spectral shape of the Ti 2p contributions are detected. However, a loss in the signal to noise ratio is clearly observed which is ascribed to the Ti (constituent of the $Ir_{74}Ti_{26}$ film) being buried due to the growth of the am-hydr-IrO_x layer. After 10 000 cycles, titanium is revealed again, suggesting that am-hydr-IrO_x is now thinner. Therefore, this allows measuring the titanium at the interface between the am-hydr-IrO_x/Ir_xTi_{1-x} stack and the underlying metallic alloy. Additionally, the titanium is further oxidized, implicitly indicating a reaction with the electrolyte.

In the pristine Ir_{100} film, iridium is in its metallic state. After 1000 cycles, photoemission lines corresponding to oxidized iridium are the only ones observed. This is interpreted as the am-hydr-IrO_x layer being significantly thicker in this sample and, therefore, no significant signal from the unreacted alloy film is detected. After 10 000 cycles the Ir 4f signal is similar to its pristine counterpart (Fig. 5d). This is interpreted as near-complete delamination of the catalytic layer, where the remaining non-oxidised iridium was electrically isolated due to loss of the conductive catalytic layer and did not participate in the growth. In addition, the strong Si 2p signal arising from the substrate onto which the film was sputtered reveals that the remaining film is very thin or does not cover the support completely (Fig. 5f). In

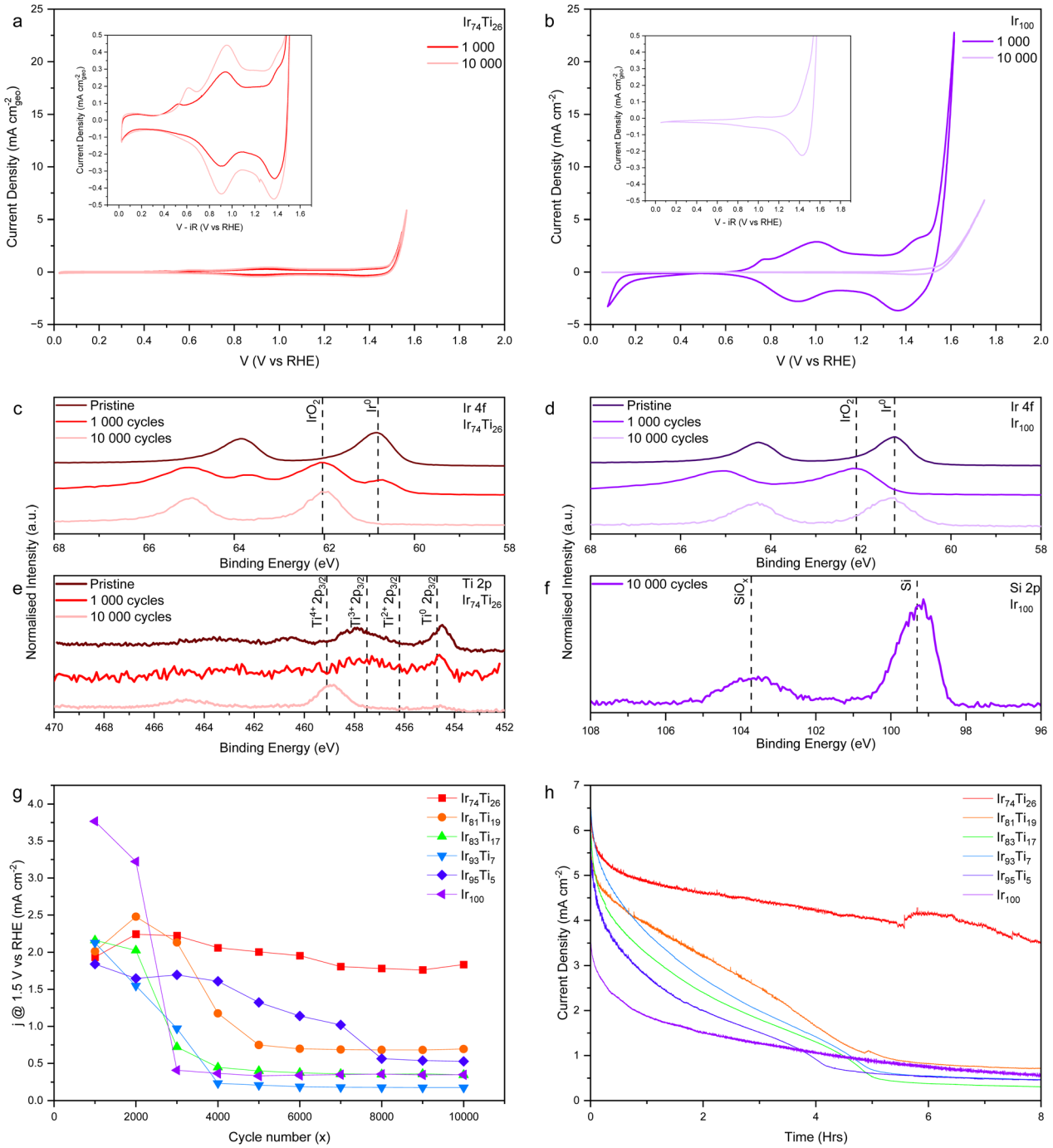

Fig. 5 Electrochemical stability of am-hydr-IrO_x grown from Ir_xTi_{100-x}: comparison of cyclic voltammograms measured after 1000 and 10 000 cycles performed on $Ir_{74}Ti_{26}$ (a) and Ir_{100} (b) films. Insets highlight changes in (pseudo)capacitance. (c) and (e) XPS/HAXPES spectra of Ir 4f and Ti 2p, respectively, comparing the pristine $Ir_{74}Ti_{26}$ alloy film with the sample after 1000 and 10 000 cycles. (d) and (f) XPS/HAXPES spectra of Ir 4f and Si 2p, respectively, comparing the pristine Ir_{100} film with the sample after 1000 and 10 000 cycles. The data of the pristine samples and after 10 000 cycles were acquired by XPS with an Al K_α source, while the data after 1000 cycles were acquired by HAXPES using 2 keV excitation photon energy. (g) Stability towards cycle-induced delamination quantified by the current density, measured at 1.5 V *vs.* RHE, as a function of cycle number. (h) Potentiostatic stability measured through chronoamperometry at 1.7 V *vs.* RHE on samples grown to 1000 cycles.

contrast, the sample grown from $Ir_{74}Ti_{26}$ shows no evidence of delamination (by means of Si peak identification as shown in Fig. S16). However, the elemental ratio of the iridium and titanium species has shifted to $Ir_{58}Ti_{42}$ (calculated as before, using the Ir 4f and Ti 2p regions). This is consistent with the maturation of the film through electrochemically driven corrosion into the electrolyte with no significant loss of electroactive area as indicated by a higher pseudo-capacitive response of the redox features. In addition, the Ti 2p spectrum of the 10 000-cycle sample in Fig. 5e shows a lower proportion of metallic titanium,

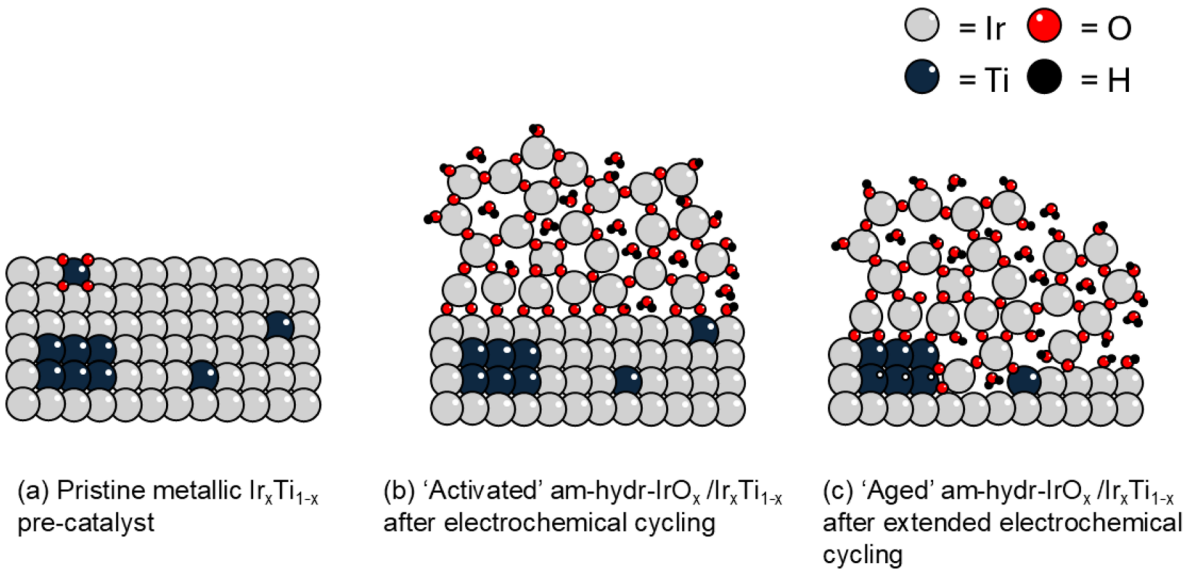

Fig. 6 Proposed model for the structural evolution of the studied samples. (a) Pristine metallic alloy film with both isolated crystal domains of titanium and titanium within the iridium matrix. Surface titanium is also partially oxidised through exposure to air. (b) 'Activated' am-hydr-IrO_x formed on the metallic substrate. (c) 'Aged' am-hydr-IrO_x, extended cycling has developed the hydrous layer deeper into the metallic substrate allowing more titanium to be accessed spectroscopically due to loss of surface iridium and allowing further oxidation of metallic titanium.

attributed to a more oxidized state, as expected after the extensive electrochemical treatment with the loss of iridium exposing the underlying titanium to the electrolyte.

Fig. 5h shows the potentiostatic stability measured through chronoamperometry at 1.7 V *vs.* RHE after the accelerated degradation tests. Fig. 5g shows the relative rate of degradation of all samples by depicting the loss in current density at 1.5 V *vs.* RHE of a given cycle number. All the high iridium content samples (Ir_{100}–Ir_{83}) show rapid degradation, likely due to the delamination of the am-hydr-IrO_x species during the test. However, samples with higher titanium content (*e.g.* $Ir_{74}Ti_{26}$) exhibit significantly slower degradation, with no profound loss of activity (*e.g.* −95% for $Ir_{74}Ti_{26}$ *vs.* −10% for Ir_{100}).

Fig. 6 illustrates the evolution of the samples through the extended cycling procedure. After 1000 cycles, the pristine metallic pre-catalyst in Fig. 6a transforms into the am-hydr-IrO_x/Ir_xTi_{1-x} layer stack, in which the underlying alloy is only spectroscopically available for the thinnest am-hydr-IrO_x layer grown from $Ir_{74}Ti_{26}$. After 10 000 cycles, the am-hydr-IrO_x layer thins, due to electrochemically enhanced corrosion leaching iridium into the electrolyte, revealing titanium that has been partially oxidised due to exposure to the electrolyte.

3. Discussion

3.1 Titanium oxide as a growth inhibitor for am-hydr-IrO_x

The complex non-homogenous chemical compositions of the IrTi alloy films were thoroughly characterised and the evolution of the electrochemically grown am-hydr-IrO_x structure was studied up to layers corresponding to 1000 grow cycles. We show that the presence of the titanium within the pristine alloy is crucial for enhancing the stability (both with respect to Ir dissolution and delamination) of the electrocatalyst by modifying the growth mechanism of am-hydr-IrO_x, resulting in a drastically lower growth rate. Additionally, profound improvements in stability are achieved with minimal loss of intrinsic activity.

XPS analysis of the sputtered IrTi films (Fig. S6 and S7) revealed that with higher total titanium content within the film, a higher relative amount of titanium oxide is observed at the surface. Electrochemical cycling induced the formation of am-hydr-IrO_x layers, whose growth rate was significantly decreased with higher initial Ti content, as evidenced by the pseudo-capacitive currents in Fig. 2.

Hard X-ray photoelectron spectroscopy (HAXPES) measurements (Fig. 3) provided critical insights into the unexpected, layered structure: at 1000 growth cycles, all samples show evidence of a stacked am-hydr-IrO_x/Ir_xTi_{1-x} layered structure, where at the surface, the electrochemically active am-hydr-IrO_x interacts with the electrolyte and electrochemically evolves oxygen. This layer is supported by the remaining unreacted IrTi alloy. Evidence from HAXPES (Fig. 3) and *operando* XAS (Fig. S15) shows that am-hydr-IrO_x grown from all IrTi alloy films differs only in thickness but not composition. Additionally, the amount of titanium in the pristine alloy correlates strongly with the impeded growth rate of am-hydr-IrO_x (Fig. 2c) and pristine samples with higher titanium content have proportionately higher titanium oxide at the surface (Fig. S6 and S7). By combining these observations, it is evident that the titanium oxide at the sample surface hinders continued growth of am-hydr-IrO_x by blocking underlying iridium from the electrolyte. After the initial 1000 growth cycles, sufficiently high concentrations of titanium oxide prevent further growth. This is in contrast to am-hydr-IrO_x grown from pure iridium, which grows continuously until eventual delamination. Although the decreased growth rate of alloys with higher Ti content results in

fewer electrochemically actives sites (as revealed by a lower voltametric charge, *i.e.* a thinner film), interestingly it does not negatively affect its OER activity as shown in Fig. 4, even with fewer participating sites. This is likely related to the unique structure of hydrous iridium oxide electrocatalysts. The authors propose that the non-linearity of the thickness–activity relationship could be explained by diffusion limitations of the electrolyte deep within the am-hydr-IrO_x structure. While the innermost parts of am-hydr-IrO_x are still electrically active and can still interact with the limited electrolyte that wets the hydrated structure, and hence exhibit measurable electrochemical redox, the local area can be partially depleted of water under operational conditions. This leads to slow H_2O diffusion, increasing mass transfer resistance and, therefore, slow O_2 generation in these areas.[34] Further work is required to more comprehensively understand these observations but this is beyond the scope of this manuscript.

Now the different chemistries of iridium and titanium can be compared to rationalise this behaviour. As iridium is stable in multiple oxidation states, it can undergo oxidation and partial reduction required to form am-hydr-IrO_x. Within the cycling potential regime between 0.05–1.5 V, TiO_2 is stable and does not undergo redox reactions.[35] Titanium particles, even on the nanoscale, are resistant to total oxidation due to the formation of a non-porous oxide layer limiting diffusion of electrolyte to underlying metallic titanium.[33] To summarise, during the growth, the oscillating voltage leads to the transformation of iridium to am-hydr-IrO_x as well as to an opening of the structure, allowing electrolyte to penetrate and react with metallic iridium at later growth cycles. Titanium, in contrast, undergoes limited surface oxidation, hindered by the formation of the non-porous oxide-based passivation layer. It is possible that the presence of the titanium oxide surface layer has the effect of shielding underlying metallic iridium from participating in the growth, leading to a am-hydr-IrO_x growth rate highly sensitive to the titanium concentration.

3.2 Further roles of titanium in stability enhancement

The stabilisation effect of titanium towards iridium dissolution (Fig. 5h) is consistent with previous reports.[24,28,36,37] This raises the question of whether it plays a similar role in the materials studied here or whether all stability improvements can be ascribed to differences in thicknesses of the am-hydr-IrO_x layer. Thickness is a key factor contributing to the stability of the am-hydr-IrO_x layer with respect to electrochemical cycling; however alternative factors may also contribute to the potentiostatic stability. Fig. 5h shows that there is a clear critical amount of titanium required in the alloy to achieve high stability in the resultant active am-hydr-IrO_x layer. This suggests that titanium may influence the stability of iridium with respect to dissolution through a different mechanism, although there is no direct evidence for the presence of titanium within the am-hydr-IrO_x. In the cases in which titanium could be detected, the am-hydr-IrO_x is thin enough that it cannot be excluded that the signal corresponds to the metallic alloy film. However, a significant stability increase with titanium content as low as 1.92% has been reported.[38] One possible explanation could be that a small and, therefore, undetected amount of titanium within the am-hydr-IrO_x reduces the iridium dissolution rate. Alternatively, since iridium is separated from the alloy when the am-hydr-IrO_x forms, another possible explanation would be the presence of a titanium-rich interlayer at the interface between the am-hydr-IrO_x/Ir_xTi_{1-x} stack. Although there is no direct experimental evidence to support this, it is supported indirectly by the observation of an increase in series resistance with respect to the initial titanium content for films grown up to 1000 cycles (Fig. 4b). Since iridium and its oxides are more electrically conductive, an increasing series resistance could be explained by titanium oxides at this interface.

To further study this, the XPS of the Ti 2p region of am-hydr-IrO_x grown on $Ir_{74}Ti_{26}$ cycled 10 000 times was deconvoluted, as shown in Fig. S17, revealing that there is still a significant amount of metallic titanium as well as suboxides of titanium which are still conductive. These results can help to explain the continued electrochemical activity with some loss of activity due to an increased resistance but without total electrical isolation of the electrochemically active layer with respect to the current collector. An analogue observation was found for co-sputtered Ir–Ti films, where Ti suboxides in the interfaces favoured the stability of the electrocatalysts without hindering its activity.[22]

With this information about the surface oxidation state of titanium, the bulk structure of the samples that had undergone 1000 electrochemical cycles was also probed by Ti K-edge XAS measurements, as well as a pristine alloy sample ($Ir_{74}Ti_{26}$) for comparison. A linear combination fitting approach of the Ti K-edge XAS spectra was performed using references of metallic titanium as well as several common titanium oxides (TiO, Ti_2O_3, Ti_4O_7 and TiO_2) as potential candidate structures for titanium within the sample. Attempts to use these structures failed to produce acceptable fits to the measured data, whereby key features of the spectra could not be reproduced as shown in Fig. S11. Additionally, all fits give large contributions of Ti_4O_7 which does not follow chemical intuition as the samples are prepared under ultra-high vacuum (UHV) conditions and have high metallic contributions at the surface. It has been shown elsewhere that when titanium alloys with other metals, charge-transfer processes can occur between the metals, leading to shifts in the observed spectra.[39] Indeed, this has already been observed for the Ir 4f XPS data of the pristine samples in Fig. 1b, in which a shift towards lower binding energies of Ir 4f is observed. This implies that electron density is moving from titanium to iridium, which corresponds well with the increase in white line position resulting from a decreased electron density around titanium. The fitting procedure was repeated with $Ir_{91}Ti_9$ as a reference (see Fig. S12), since in this sample the titanium is too diluted to form a significant number of isolated structures within the alloy and, therefore, is representative of the IrTi solid solution. The results show that with more titanium in the structure, increasing contributions of Ti and TiO_2 are observed within the fit, which agrees well with previous characterisation. To summarise, after 1000 cycles the unreacted underlying alloy film layer dominates the signal and the electronic state of the layers is best described as a metallic alloy between iridium and titanium, with increasing amounts of isolated titanium at high titanium content.

4. Conclusion

This study provides detailed insights into a strategy for improving the stability of am-hydr-IrO_x electrocatalysts without the typical accompanying loss of activity leading to a promising PEM anode material exhibiting both high activity and stability. By utilizing both lab-based and synchrotron-based spectroscopic techniques, snapshots of the evolving electrocatalyst structure were obtained. Most importantly, it has been shown that the presence of Ti in the initial Ir matrix hinders the growth of am-hydr-IrO_x. This fact can be used to tune the stability of these film materials by controlling the amount of metallic iridium in the underlying film consumed during the electrochemical growth. The mechanical stability of these films highly depends on the presence of some remaining Ir to anchor the electrocatalyst. Within the pristine samples with higher surface titanium content, there is clear evidence of a higher relative amount of titanium oxide. The am-hydr-IrO_x growth dynamics are highly sensitive to the amount of titanium oxide and above a critical concentration, a profound improvement in electrochemical stability is observed.

Conflicts of interest

There are no conflicts to declare.

Data availability

The raw data utilised in this work have been deposited online in a Zenodo repository that has the following permanent DOI: https://doi.org/10.5281/zenodo.18164742.

Supplementary information (SI) is available. See DOI: https://doi.org/10.1039/d6ta03607d.

Acknowledgements

This project was funded by the German Federal Ministry of Education and Research (Bundesministerium für Bildung und Forschung, BMBF) under Grant No. 03 EW0015B (CatLab). The authors acknowledge and appreciate the administrative coordinating role of Dr. Steffi Hlawenka for this project. The HZB is gratefully acknowledged for granting access to the synchrotron radiation facility BESSY II (for HAXPES and XAS measurements at HiKE) and the Energy Materials *In situ* Laboratory Berlin (EMIL, for sample preparation and lab-based XPS measurements). The authors thank the ALBA Synchrotron (Cerdanyola del Vallès, Barcelona, Spain) for beamtime allocation at the BL16-NOTOS beamline (proposal n° 2022097090) and the ALBA staff for their support.

Notes and references

1 S. Krishnan, *et al.*, Present and future cost of alkaline and PEM electrolyser stacks, *Int. J. Hydrogen Energy*, 2023, **48**, 32313–32330.
2 A. H. Reksten, M. S. Thomassen, S. Møller-Holst and K. Sundseth, Projecting the future cost of PEM and alkaline water electrolysers; a CAPEX model including electrolyser plant size and technology development, *Int. J. Hydrogen Energy*, 2022, **47**, 38106–38113.
3 Y. Xie, F. Luo and Z. Yang, Strategies for the enhancements in catalytic performance and stability of anodic electrocatalyst in PEM water splitting, *Energy Rev.*, 2024, **3**, 100103.
4 International Energy Agency (IEA), *Electrolysers*, https://www.iea.org/energy-system/hydrogen/electrolysers, accessed 2023.
5 L. She, *et al.*, On the Durability of Iridium-Based Electrocatalysts toward the Oxygen Evolution Reaction under Acid Environment, *Adv. Funct. Mater.*, 2022, **32**, 2108465.
6 R. V. Mom, *et al.*, Operando Structure–Activity–Stability Relationship of Iridium Oxides during the Oxygen Evolution Reaction, *ACS Catal.*, 2022, **12**, 5174–5184.
7 O. Kasian, J.-P. Grote, S. Geiger, S. Cherevko and K. J. J. Mayrhofer, The Common Intermediates of Oxygen Evolution and Dissolution Reactions during Water Electrolysis on Iridium, *Angew. Chem., Int. Ed.*, 2018, **57**, 2488–2491.
8 L. Böhm, *et al.*, Pulsed electrodeposition of iridium catalyst nanoparticles on titanium suboxide supports for application in PEM electrolysis, *Mater. Today Proc.*, 2021, **45**, 4254–4259.
9 A. Weiß, *et al.*, Impact of Intermittent Operation on Lifetime and Performance of a PEM Water Electrolyzer, *J. Electrochem. Soc.*, 2019, **166**, F487.
10 P. J. Rheinländer and J. Durst, Transformation of the OER-Active IrO_x Species under Transient Operation Conditions in PEM Water Electrolysis, *J. Electrochem. Soc.*, 2021, **168**, 024511.
11 S. Cherevko, S. Geiger, O. Kasian, A. Mingers and K. J. J. Mayrhofer, Oxygen evolution activity and stability of iridium in acidic media. Part 1. – Metallic iridium, *J. Electroanal. Chem.*, 2016, **773**, 69–78.
12 S. Cherevko, S. Geiger, O. Kasian, A. Mingers and K. J. J. Mayrhofer, Oxygen evolution activity and stability of iridium in acidic media. Part 2. – Electrochemically grown hydrous iridium oxide, *J. Electroanal. Chem.*, 2016, **774**, 102–110.
13 J. Mozota and B. E. Conway, Surface and bulk processes at oxidized iridium electrodes—I. Monolayer stage and transition to reversible multilayer oxide film behaviour, *Electrochim. Acta*, 1983, **28**, 1–8.
14 B. E. Conway and J. Mozota, Surface and bulk processes at oxidized iridium electrodes—II. Conductivity-switched behaviour of thick oxide films, *Electrochim. Acta*, 1983, **28**, 9–16.
15 V. I. Birss, C. Bock and H. Elzanowska, Hydrous Ir oxide films: the mechanism of the anodic prepeak reaction, *Can. J. Chem.*, 1997, **75**, 1687–1693.
16 D. N. Buckley and L. D. Burke, The oxygen electrode. Part 6.—Oxygen evolution and corrosion at iridium anodes, *J. Chem. Soc. Faraday. Trans.*, 1976, **1**(72), 2431–2440.

17 V. Birss, R. Myers, H. Angerstein-Kozlowska and B. E. Conway, Electron Microscopy Study of Formation of Thick Oxide Films on Ir and Ru Electrodes, *J. Electrochem. Soc.*, 1984, **131**, 1502–1510.
18 H. Li, *et al.*, Stability of electrocatalytic OER: from principle to application, *Chem. Soc. Rev.*, 2024, **53**, 10709–10740.
19 A. Lončar, D. Escalera-López, S. Cherevko and N. Hodnik, Inter-relationships between Oxygen Evolution and Iridium Dissolution Mechanisms, *Angew. Chem., Int. Ed.*, 2022, **61**, e202114437.
20 M. Van Der Merwe, *et al.*, Unravelling the mechanistic complexity of the oxygen evolution reaction and Ir dissolution in highly dimensional amorphous hydrous iridium oxides, *Energy Environ. Sci.*, 2025, **18**, 1214–1231.
21 R. D. Meyer, S. F. Cogan, T. H. Nguyen and R. D. Rauh, Electrodeposited iridium oxide for neural stimulation and recording electrodes, *IEEE Trans. Neural Syst. Rehabil. Eng.*, 2001, **9**, 2–11.
22 M. D. Obradović, B. D. Balanč, U. Č. Lačnjevac and S. Lj. Gojković, Electrochemically deposited iridium-oxide: Estimation of intrinsic activity and stability in oxygen evolution in acid solution, *J. Electroanal. Chem.*, 2021, **881**, 114944.
23 M. van der Merwe, *et al.*, The Chemical and Electronic Properties of Stability-Enhanced, Mixed Ir-TiOx Oxygen Evolution Reaction Catalysts, *ACS Catal.*, 2023, **13**, 15427–15438.
24 O. Kasian, *et al.*, Stabilization of an iridium oxygen evolution catalyst by titanium oxides, *J. Phys.: Energy*, 2021, **3**, 034006.
25 O. Kasian, *et al.*, Using Instability of a Non-stoichiometric Mixed Oxide Oxygen Evolution Catalyst As a Tool to Improve Its Electrocatalytic Performance, *Electrocatalysis*, 2018, **9**, 139–145.
26 G. Li, *et al.*, Iridium-Tin oxide solid-solution nanocatalysts with enhanced activity and stability for oxygen evolution, *J. Power Sources*, 2016, **325**, 15–24.
27 E. Oakton, *et al.*, IrO_2-TiO_2: A High-Surface-Area, Active, and Stable Electrocatalyst for the Oxygen Evolution Reaction, *ACS Catal.*, 2017, **7**, 2346–2352.
28 M. Frisch, *et al.*, ALD-Coated Mesoporous Iridium-Titanium Mixed Oxides: Maximizing Iridium Utilization for an Outstanding OER Performance, *Adv. Mater. Interfaces*, 2022, **9**, 2102035.
29 I. Hacisalihoglu, A. Samancioglu, F. Yildiz, G. Purcek and A. Alsaran, Tribocorrosion properties of different type titanium alloys in simulated body fluid, *Wear*, 2015, **332–333**, 679–686.
30 Y. Nakaya and S. Furukawa, Catalysis of Alloys: Classification, Principles, and Design for a Variety of Materials and Reactions, *Chem. Rev.*, 2023, **123**, 5859–5947.
31 M. Gorgoi, *et al.*, The high kinetic energy photoelectron spectroscopy facility at BESSY progress and first results, *Nucl. Instrum. Methods Phys. Res., Sect. A*, 2009, **601**, 48–53.
32 B. L. Henke, E. M. Gullikson and J. C. Davis, X-Ray Interactions: Photoabsorption, Scattering, Transmission, and Reflection at E = 50-30,000 eV, Z = 1-92, *At. Data Nucl. Data Tables*, 1993, **54**, 181–342.
33 H. Garbacz, M. Pisarek and K. J. Kurzydłowski, Corrosion resistance of nanostructured titanium, *Biomol. Eng.*, 2007, **24**, 559–563.
34 P. Steegstra, M. Busch, I. Panas and E. Ahlberg, Revisiting the Redox Properties of Hydrous Iridium Oxide Films in the Context of Oxygen Evolution, *J. Phys. Chem. C*, 2013, **117**, 20975–20981.
35 E. McCafferty, Thermodynamics of Corrosion: Pourbaix Diagrams. in *Introduction to Corrosion Science*, ed. E. McCafferty, Springer, New York, NY, 2010, pp. 95–117, DOI: 10.1007/978-1-4419-0455-3_6.
36 A. Touni, *et al.*, Iridium oxide-nickel-coated titanium anodes for the oxygen evolution reaction, *Electrochim. Acta*, 2021, **390**, 138866.
37 S. Cherevko, *et al.*, Stability of nanostructured iridium oxide electrocatalysts during oxygen evolution reaction in acidic environment, *Electrochem. Commun.*, 2014, **48**, 81–85.
38 Y. Wang, *et al.*, Inverse doping IrO_x/Ti with weakened Ir-O interaction toward stable and efficient acidic oxygen evolution, *Chem*, 2023, **9**, 2931–2942.
39 A. Bzowski and T. K. Sham, Pd-Ti bimetallics: A study of the electronic structure using x-ray photoelectron spectroscopy and x-ray-absorption near-edge structure, *Phys. Rev. B:Condens. Matter Mater. Phys.*, 1993, **48**, 7836–7840.